Modeling of mixed-mode debonding in the peel test applied to superficial reinforcements

Fourth International Conference on FRP Composites in Civil Engineering (CICE2008)
22-24July 2008, Zurich, Switzerland

Modeling of mixed-mode debonding in the peel test applied to superficial reinforcements

L. De Lorenzis, G. Zavarise
Department of Innovation Engineering, Università del Salento, Lecce, Italy

ABSTRACT: This paper focuses on modeling of the interface between a rigid substrate and a thin elastic adherend subjected to mixed-mode loading in the peel test configuration. The problem is approached both analytically and numerically. The analytical model is based on linear-elastic fracture mechanics. In the numerical model, the interface is modeled with contact elements which take into account both debonding and contact using the node-to-segment contact strategy. Uncoupled cohesive interface laws are adopted in the normal and tangential directions. The models are able to predict the response of the bonded joint as a function of the main parameters. The main objective is to compute the debonding load and the effective bond length of the adherend as functions of the peel angle.

1 INTRODUCTION

The mechanics of bond between a thin plate and a flat quasi-brittle substrate, e.g., a Fiber-Reinforced Polymer (FRP) laminate and concrete, under mode-II (i.e. pure shear) loading has been clarified by extensive investigations. On the other hand, the contemporary presence of mode-II and mode-I (i.e. pure peel) loading, also defined as mixed-mode condition, takes place in several cases. Examples are the interface between FRP and substrate in the proximity of inclined cracks or at the edge of the FRP plate (Yao et al., 2005, Pan & Leung, 2006).

The so-called peel-test has been widely used to characterize the bond behavior of adhesives (Williams 1997). In this test a thin plate is pulled from the substrate at a certain angle (the "peel angle") and the "peel force" needed to produce debonding is measured (Fig. 1). The interface is subjected to shear and normal stresses, hence debonding occurs by mixed-mode fracture. Several elastic analyses show that interfacial stresses are highly localized in the vicinity of the loaded end, and that the interfacial normal stresses can be large compared with the shear stresses. After an initial focus on stress analyses, fracture mechanics has become fully established (Kim & Aravas 1988, Williams 1997). Recent studies adopt cohesive zone modeling, which bridges the gap between the two approaches (Wei & Hutchinson 1998). Despite the wide literature on the peel test, the mixed-mode effects have received a limited attention. Modeling has often assumed single-mode dominance, using a global mode-I energy balance. However, if the peel angle is small, mode mixity cannot be neglected.

Few studies, mostly of experimental nature, have addressed the bond of FRP to concrete under mixed-mode loading (see Karbhari et al. 1997, Dai et al. 2004, Pan & Leung 2007). They show that there may be a detrimental effect of the mode-I component on the debonding load, and that the Effective Bond Length (EBL) is shorter for interfaces under mixed-mode loading.

This paper focuses on modeling of the interface between a rigid substrate and a thin elastic adherend subjected to inclined loading in the peel test configuration. The main objective is to compute the debonding load of the adherend and its EBL as functions of the peel angle, in order to evaluate the effect of mode mixity on the interfacial strength. The study deals with small peel angles. The problem is approached analytically, using linear-elastic fracture mechanics (LEFM), and numerically, with the cohesive-zone modeling approach.

2 LEFM ANALYSIS OF THE PEEL TEST

In LEFM, the degree of mode mixity is typically expressed by the phase angle ψ (Thouless & Jensen 1992)

$$\psi = \tan^{-1}\sqrt{G_{II}/G_I} \tag{1}$$

where G_I and G_{II} are the mode-I and mode-II components of the energy release rate, respectively. The simplest possible mixed-mode fracture criterion is as follows

$$G_I/G_{If} + G_{II}/G_{IIf} = 1 \tag{2}$$

where G_{If} and G_{IIf} are the fracture energies in pure mode-I and mode-II conditions, respectively. Consider a thin plate of thickness t and unit width, made of a linearly elastic material with modulus E, bonded to a flat rigid substrate, and loaded with a force F at an angle θ from the horizontal (Fig. 1a). For this case, referring to Figure 1b, G_I and G_{II} can be expressed as follows

$$G_I = F_0^2/2Et \quad G_{II} = 6M_0^2/Et^3 \tag{3}$$

where F_0 and M_0 are given by (Thouless & Jensen 1992)

$$F_0 = F\cos\theta \quad M_0 = \sqrt{\frac{Et^3}{6}\left[\frac{F^2\sin^2\theta}{2Et} + F\left(1-\cos\theta\right)\right]} \tag{4}$$

Introducing eq. (4) and eq. (3) in eq. (1), the phase angle is given by

$$\psi = \tan^{-1}\left[tF_0/\sqrt{12}M_0\right] = \tan^{-1}\left[\cos\theta/\sqrt{\sin^2\theta + 2\left(1-\cos\theta\right)\frac{Et}{F}}\right] \tag{5}$$

Also, a simple way of determining the steady-state peeling load, F_{peel}, is to substitute eq. (4) into eq. (3), and combine these with eq. (2). The following expression is then obtained

$$\frac{F_{peel}}{G_{If}} = \left[\sqrt{\left(\frac{Et}{G_{If}}\right)^2\left(1-\cos\theta\right)^2 + 2\frac{Et}{G_{If}}\left(\sin^2\theta + \frac{\cos^2\theta}{r}\right)} - \frac{Et}{G_{If}}\left(1-\cos\theta\right)\right] \Big/ \left(\sin^2\theta + \frac{\cos^2\theta}{r}\right) \tag{6}$$

where F has been replaced with F_{peel}, and $r = G_{IIf}/G_{If}$. Eq. (6) shows that F_{peel}/G_{If} depends on Et/G_{If}, r and the peel angle θ. The phase angle at peeling, ψ_{peel}, is given by eq. (5) for $F = F_{peel}$

$$\psi_{peel} = \tan^{-1}\left[\cos\theta/\sqrt{\sin^2\theta + 2\left(1-\cos\theta\right)\frac{G_{If}}{F_{peel}}\frac{Et}{G_{If}}}\right] \tag{7}$$

3 NUMERICAL MODELING OF THE PEEL TEST

Different approaches have been used in the literature for cohesive zone modeling of interfaces under mixed-mode conditions (De Lorenzis & Zavarise 2008). In this paper uncoupled cohesive laws are adopted in the normal and tangential directions. Tension relates the normal relative displacement, $g_N > 0$, and the normal stress, p_N, while shear relates the tangential relative displacement, g_T, and the shear stress, p_T. This choice is made to enable the use of different values for the mode-I and mode-II interfacial fracture energies, in agreement with the experimental evidence. In compression, i.e. for $g_N < 0$, non-penetration is enforced using the penalty method.

The cohesive laws are taken as bilinear (Fig. 2). This simple model is able to capture the main characteristic parameters of the interface, hence it is often used to model the bond behavior of FRP to concrete. The energy release rates in each mode are identified as the areas under the respective cohesive laws integrated up to the current g_N and g_T, and the mixed-mode

failure criterion in eq. (2) is assumed. Once the failure criterion is met for an element under tension, the element is assumed to be no longer capable to bear any load. In compression, the behavior is the classical one of a contact element.

The above contact and cohesive models have been implemented into a contact element based on the node-to-segment strategy (Wriggers et al. 1998) and generalized to handle cohesive forces in the normal and tangential directions. The adherend is modeled with finite deformation, linearly-elastic beam elements. The substrate is discretized with 4-node isoparametric plane stress elastic elements. The non-linear problem is solved with a Newton-Raphson implicit procedure, where the tangent stiffness matrix is obtained through consistent linearization. The model is implemented in the finite element code FEAP (courtesy of Prof. R.L. Taylor).

Using dimensional analysis, the steady-state peeling load can be expressed as follows

$$F_{peel} / G_{If} = f\left(Et / G_{If}, L / t, G_{IIf} / G_{If}, p_{N\max} / E, p_{T\max} / E, \theta\right) \tag{8}$$

where L is the bond length. In our case the reference values for the parameters are: $G_{If} = 0.1\ N/mm$, $G_{IIf} = 0.4\ N/mm$, $p_{N\max} = 2\ MPa$, $p_{T\max} = 4\ MPa$, $E = 250\ GPa$, $t = 0.165\ mm$, $L = 100\ mm$. The values of g_{Nu} and g_{Tu} are, respectively $0.1\ mm$ and $0.2\ mm$. Also, $g_{N\max}/g_{Nu}$ and $g_{T\max}/g_{Tu}$ are assumed equal to 0.1. The peel angle is varied between $0°$ and $10°$.

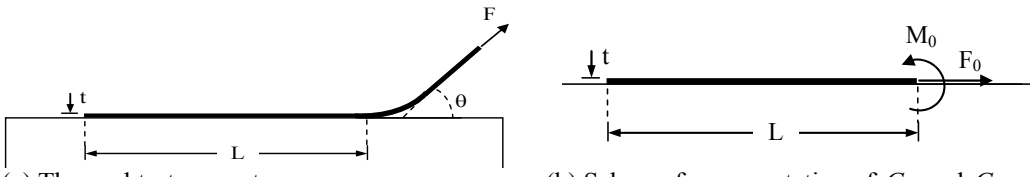

(a) The peel test geometry (b) Scheme for computation of G_I and G_{II}

Figure 1. Scheme of the peel test.

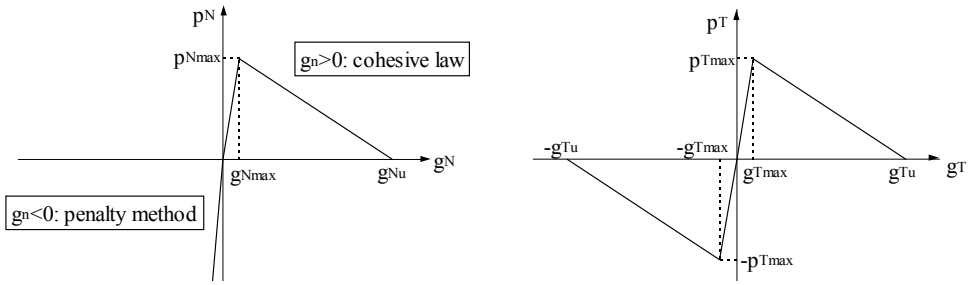

(a) Normal case (b) Tangential case

Figure 2. Relationships between interfacial tractions and relative displacements.

4 RESULTS

4.1 *Effect of the peel angle*

Figure 3a shows that the dimensionless steady-state peeling load, F_{peel} / G_{If}, decreases rapidly as the peel angle increases. The solid curves correspond to pure mode I and mode II (De Lorenzis & Zavarise 2008), whereas the dots are predictions of the numerical model. The dashed curve represents predictions of eq. (6), which are in excellent agreement with numerical results. Both results show a gradual transition from the mode-II to the mode-I curve as θ increases, in accordance with the variation of the mode mixity at failure. Figure 3b shows the phase angle predicted by eq. (7). This equals $90°$ (pure mode II) for $\theta = 0°$ and decreases rapidly with increasing peel angle, reaching about $4°$ (close to pure mode I) for $\theta = 10°$.

Figure 4 shows the interfacial stress distributions. The bonded joint moves from an *elastic stage*, where normal and shear stresses are within the first branch of the respective cohesive laws (Figs. 4a, d), through an *elastic-softening stage*, where part of the bond length is subjected to interfacial stresses within the second branch of the cohesive law (Figs. 4b, e), to an *elastic-softening-debonding stage*, where a portion of the bond length has debonded (Figs. 4c, f). Due to the existence of two cohesive laws, the interface may be at different stages in the normal and

tangential directions. However, the steady-state peeling phase invariably corresponds to the elastic-softening-debonding stage in both directions. In this phase, and in presence of a sufficiently long bond length, the interfacial stress profiles remain constant and translate from the loaded end to the free end of the joint as more contact elements sequentially reach failure.

For $\theta = 0°$ (not shown for brevity) the interface is subjected to shear stresses only. For $\theta = 2°$ (Figs. 4a-c), mode-I and mode-II energy release rates have comparable magnitude. Failure of the bonded element is attained when the energy release rates reach the boundary of the assumed domain (see eq. (2)), as shown by the abrupt drop in interfacial stresses in Fig. 4c. For $\theta = 10°$ (Figs. 4d-f), although shear stresses exist, the mode-I energy release rate is largely dominant.

The distribution of the normal stresses is more localized in the proximity of the loaded end than that of the shear stresses. As the peel angle increases, normal stresses increase and shear stresses decrease, hence the interfacial stress distributions become increasingly localized in the vicinity of the loaded end. This applies to all stages of loading of the interface.

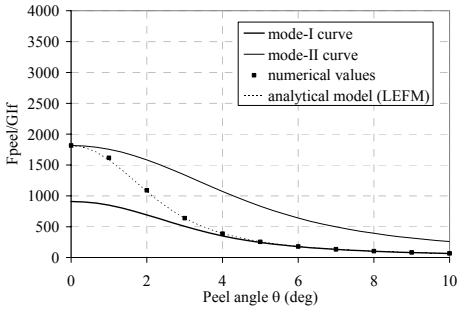

(a) Effect on the steady-state peeling load

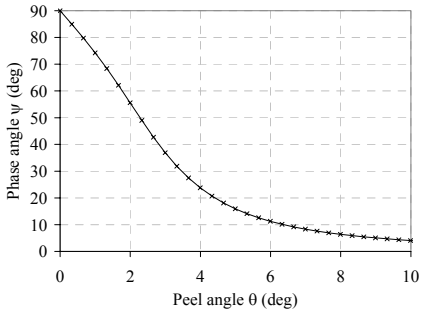

(b) Effect on the phase angle

Figure 3. Effect of the peel angle.

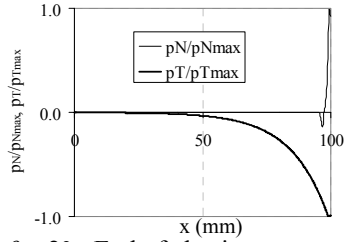

(a) $\theta = 2°$ - End of elastic stage

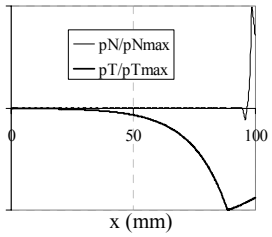

(b) $\theta = 2°$ - Elastic–soft. stage

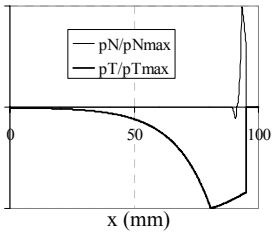

(c) $\theta = 2°$ Elastic–soft.–deb. stage

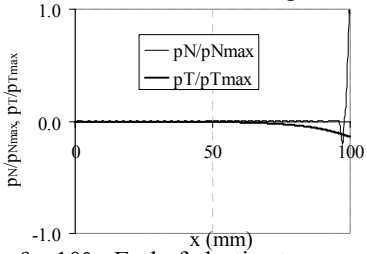

(d) $\theta = 10°$ - End of elastic stage

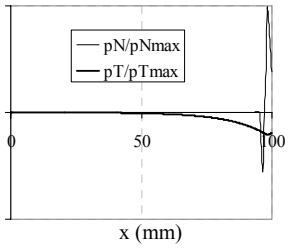

(e) $\theta = 10°$ - Elastic–soft. stage

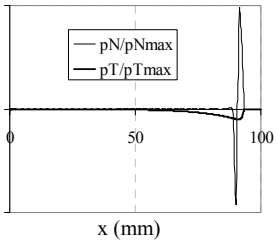

(f) $\theta = 10°$ Elastic–soft.–deb. stage

Figure 4. Interfacial stresses and energy release rates along the bond length.

4.2 *Effect of the bond length*

Numerical results show that the concept of EBL can be extended to mixed-mode conditions (De Lorenzis & Zavarise 2008). The EBL is seen to decrease as the peel angle increases (Fig. 5c), in agreement with the test results by Dai et al. (2004). This is easily explained considering that, as observed earlier, larger peel angles yield a more localized distribution of interfacial stresses. Hence a smaller bond length is needed to "accommodate" the interfacial stress profile corresponding to steady-state peeling. The characteristic lengths of the problem in mode I and mode II can be computed as follows

$$l_{ch,I} = EG_{If} / p_{N\max}^2 \quad l_{ch,II} = EG_{IIf} / p_{T\max}^2 \tag{9}$$

For the reference values of the parameters, it is $l_{ch,I} = l_{ch,II} = 6250\ mm$, hence they are considerably larger than the maximum dimension involved in the problem, i.e. the joint length. This does not prevent the numerical results from being in excellent agreement with predictions of LEFM. These continue to be valid provided that the bond length is larger than the EBL. It is shown in the following that the latter plays in this case the role of the characteristic length.

4.3 *Effect of* Et / G_{If}

For the reference values of the parameters, $Et / G_{If} = 4.13E05$. The effect of this variable is analyzed by modifying its value to $1.03E05$ and $1.65E06$. Note that as G_{IIf} / G_{If} is constant, Et / G_{If} and Et / G_{IIf} vary by the same proportion. Figure 5a shows that the trend of the steady-state peeling load vs. the peel angle remains similar, and once again there is excellent agreement between analytical and numerical predictions. As Et / G_{If} increases, the mode-I curve is approached faster. This is shown by Fig. 5b, where the phase angle decreases at a faster rate as Et / G_{If} increases.

Note that the numerical steady-state peeling loads reported in Fig. 5 have all been obtained for lengths of the bonded joint larger than the EBLs at the respective peel angles. Once again, provided that this condition is satisfied, LEFM predictions continue to hold.

The EBL decreases as the Et / G_{If} ratio increases (Fig. 5c). Increasing Et / G_{If} corresponds to increasing the axial stiffness of the adherend or, equivalently, to decreasing the fracture energy. For given cohesive strengths, this implies increasing the stiffness of the interface in both mode I and mode II. This in turn yields a more localized distribution of cohesive stresses and hence a smaller EBL. The decrease of the EBL is particularly pronounced for small peel angles, where the EBL is larger due to the predominant influence of the shear stresses.

The characteristic lengths vary linearly with the Et / G_{If} ratio, hence they are equal to $1562.5\ mm$ for $Et / G_{If} = 1.03E05$, and to $25000\ mm$ for $Et / G_{If} = 1.65E06$. The results above show that the variation of the EBL follows the trend of the variation of the characteristic lengths. In this case, both $l_{ch,I}$ and $l_{ch,II}$ vary at the same time. Hence it is not possible to correlate the EBL to one characteristic length in particular.

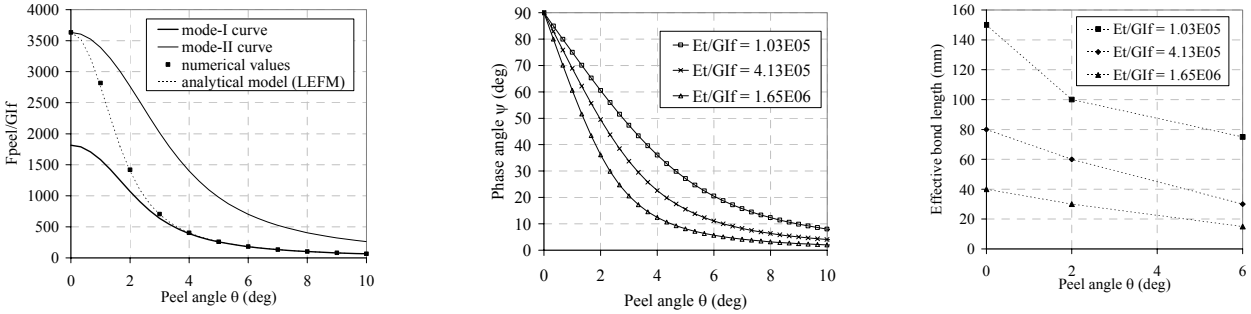

(a) F_{peel} vs. θ for $Et / G_{If} = 1.65E06$ (b) Effect of Et / G_{If} on the phase angle (c) Effect of Et / G_{If} on the EBL

Figure 5. Effect of the Et / G_{If} ratio.

4.4 *Effect of* $p_{T\max} / E$ *and* $p_{N\max} / E$

The effect of $p_{T\max} / E$ and $p_{N\max} / E$ is analyzed by modifying $p_{T\max}$ to $1\ MPa$ and $16\ MPa$, and $p_{N\max}$ to $0.5\ MPa$ and $8\ MPa$. The steady-state peeling load is weakly influenced by the cohesive strengths (De Lorenzis & Zavarise 2008). Conversely, the effect on the EBL may result significant (Fig. 6). Decreasing $p_{T\max} / E$ ($p_{N\max} / E$) corresponds to increasing the ultimate tangential (normal) gap at the interface, which in turn implies a decrease (in absolute value) of the slopes of both branches of the mode-II (mode-I) cohesive law. As the interface becomes more deformable, the effect is similar to increasing the axial stiffness of the adherend, hence the effects on the interfacial stress distributions are similar to those obtained increasing Et / G_{If}, but they are limited to the mode-II (mode-I) response.

Since the shear stresses involve a larger portion of the joint than the normal stresses, they control the EBL. As a result, the EBL increases when $p_{T\max} / E$ decreases (Fig. 6a). The effect is more pronounced for small peel angles, for which mode II is prevalent. Note that, as $p_{T\max} / E$

decreases 4 times, $l_{ch,II}$ increases 16 times while $l_{ch,I}$ is unchanged. Hence, the variation of the EBL follows that of $l_{ch,II}$. Conversely, since the normal stresses involve a shorter portion of the joint length, they have almost no influence on the EBL. As a result, a small effect of $p_{N\max}/E$ on the EBL is only observed for the largest peel angle analyzed, for which mode I is prevalent (Fig. 6b). As $p_{N\max}/E$ decreases 4 times, $l_{ch,I}$ increases 16 times while $l_{ch,II}$ remains unchanged. Hence there is a weak relationship between the variation of $l_{ch,I}$ and that of the EBL, as the latter is mainly controlled by the shear stress distribution. Obviously, as the peel angle increases and pure mode-I conditions are approached, the EBL will be related to $l_{ch,I}$ more than to $l_{ch,II}$.

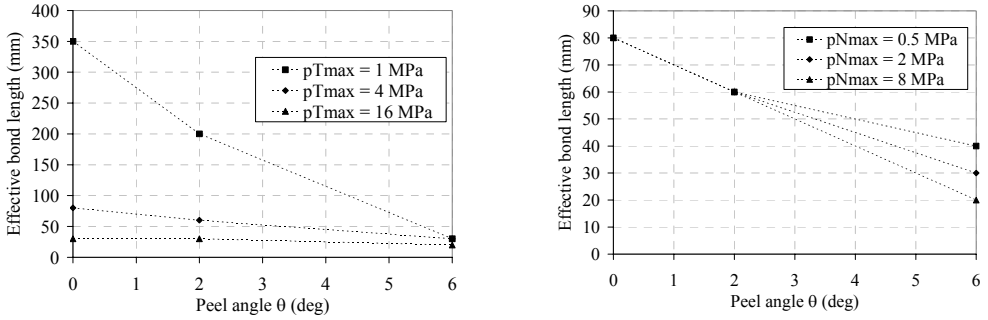

(a) Variable $p_{T\max}$, $p_{N\max} = 2\ MPa$ (b) Variable $p_{N\max}$, $p_{T\max} = 4\ MPa$

Figure 6. Effect of the cohesive strengths $p_{T\max}$ and $p_{N\max}$ on the EBL.

5 CONCLUSIONS

This paper has focused on modeling of the interface between a rigid substrate and a thin elastic adherend subjected to inclined loading in the peel test configuration. An excellent agreement is found between numerical predictions based on cohesive-zone modeling, and analytical predictions based on LEFM, provided that the length of the joint is larger than its EBL. Despite their simplicity, the models appear capable of interpreting various aspects of the physical behavior effectively, namely the distribution of interfacial stresses along the bond length, and the variation with the peel angle of the debonding load, of the degree of mode mixity and of the EBL.

6 REFERENCES

Dai, J.G., Ueda, T., Sato, Y. & Hadiyono, J. 2004. Dowel resistances of bond interfaces between FRP sheets and concrete. *Proc. of the Second CICE Conference*, Adelaide, Australia, 371-379.

De Lorenzis, L., and Zavarise, G. 2008. Modeling of mixed-mode debonding in the peel test applied to superficial reinforcements. *International Journal of Solids and Structures*, submitted.

Karbhari, V.M., Engineer, M., and Eckel II, D.A. 1997. On the durability of composite rehabilitation schemes for concrete: use of a peel test. *Journal of Materials Science*, 32: 147-156.

Kim, K.S., & Aravas, N. 1988. Elastoplastic analysis of the peel test. *International Journal of Solids and Structures*, 24 (4): 417-435.

Pan, J., & Leung, C.K.Y. 2007. Debonding along the FRP-concrete interface under combined pulling/peeling effects. *Engineering Fracture Mechanics*, 74: 132-150.

Thouless, M. D. & Jensen, H. M. 1992. Elastic Fracture Mechanics of the Peel-Test Geometry. *Journal of Adhesion*, 38: 185-197.

Wei, Y., & Hutchinson, J.W. 1998. Interface strength, work of adhesion and plasticity in the peel test. *International Journal of Fracture*, 93: 315-333.

Williams, J.G. 1997. Energy release rate for the peeling of flexible membranes and the analysis of blister tests. *International Journal of Fracture*, 87: 265-288.

Wriggers, P., Zavarise, G., & Zohdi, T.I. 1998. A computational study of interfacial debonding damage in fibrous composite materials. *Computational Materials Science*, 12: 39-56.

Yao, J., Teng, J.G., & Chen, J.F. 2005. Experimental study on FRP-to-concrete bonded joints. *Composites: Part B*, 36: 99-113.